



# Exosomes derived from cyclic mechanical stretch-exposed bone marrow mesenchymal stem cells inhibit RANKL-induced osteoclastogenesis through the NF- $\kappa$ B signaling pathway

Fei Xiao<sup>1#</sup>, Bin Zuo<sup>1#</sup>, Bo Tao<sup>2#</sup>, Chuandong Wang<sup>1</sup>, Yang Li<sup>1</sup>, Jianping Peng<sup>1</sup>, Chao Shen<sup>1</sup>, Yiming Cui<sup>1</sup>, Junfeng Zhu<sup>1</sup>, Xiaodong Chen<sup>1</sup>

<sup>1</sup>Department of Orthopedic Surgery, Xinhua Hospital Affiliated to Shanghai Jiao Tong University School of Medicine (SJTUSM), Shanghai, China;

<sup>2</sup>Department of Orthopedics, Tianjin Medical University General Hospital, Tianjin, China

**Contributions:** (I) Conception and design: F Xiao, B Zuo, B Tao; (II) Administrative support: X Chen; (III) Provision of study materials or patients: F Xiao, X Chen; (IV) Collection and assembly of data: F Xiao, B Zuo, B Tao; (V) Data analysis and interpretation: F Xiao, B Zuo, B Tao; (VI) Manuscript writing: All authors; (VII) Final approval of manuscript: All authors.

<sup>#</sup>These authors contributed equally to this work.

**Correspondence to:** Junfeng Zhu. Department of Orthopedic Surgery, Xinhua Hospital Affiliated to Shanghai Jiao Tong University School of Medicine, 1665 Kongjiang Road, Shanghai, China. Email: zhujunfeng@xinhumed.com.cn; Xiaodong Chen. Department of Orthopedic Surgery, Xinhua Hospital Affiliated to Shanghai Jiao Tong University School of Medicine, 1665 Kongjiang Road, Shanghai, China. Email: chenxiaodong@xinhumed.com.cn.

**Background:** Skeletal unloading usually induces severe disuse osteoporosis (DOP), which often occurs in patients subjected to prolonged immobility or in spaceflight astronauts. Increasing evidence suggests that exosomes are important mediators in maintaining the balance between bone formation and resorption. We hypothesized that exosomes play an important role in the maintenance of bone homeostasis through intercellular communication between bone marrow mesenchymal stem cells (BMSCs) and osteoclasts under mechanical loading.

**Methods:** Cells were divided into cyclic mechanical stretch (CMS)-treated BMSCs and normal static-cultured BMSCs, and exosomes were extracted by ultracentrifugation. After incubation with CMS-treated BMSC-derived exosomes (CMS\_Exos) or static-cultured BMSC-derived exosomes (static\_Exos), the apoptosis rates of bone marrow macrophages (BMMs) were determined by flow cytometry, and cell viability was detected with a Cell Counting Kit-8 (CCK-8) assay. Osteoclast differentiation was determined with an *in vitro* osteoclastogenesis assay. Signaling pathway activation was evaluated by western blotting and immunofluorescence staining. Hindlimb unloading (HU)-induced DOP mouse models were prepared to evaluate the function of exosomes in DOP.

**Results:** Both CMS\_Exos and static\_Exos could be internalized by BMMs, and CMS\_Exos did not affect BMM viability or increase apoptosis. The CMS\_Exos effectively suppressed receptor activator of nuclear factor kappa-B ligand (RANKL)-mediated osteoclastogenesis and F-actin ring formation. Further molecular investigation demonstrated that CMS\_Exos impaired osteoclast differentiation via inhibition of the RANKL-induced nuclear factor kappa-B (NF- $\kappa$ B) signaling pathway. Both CMS\_Exos and static\_Exos partly rescued the osteoporosis caused by mechanical unloading; however, the CMS\_Exo group showed more obvious rescue. Treatment with CMS\_Exos significantly decreased the number of tartrate-resistant acid phosphatase (TRAP)-positive osteoclasts. Exosomes derived from CMS-treated BMSCs strongly inhibited osteoclast differentiation by attenuating the NF- $\kappa$ B signaling pathway *in vitro* and rescued osteoporosis caused by mechanical unloading in an HU mouse model *in vivo*.

**Conclusions:** In this research, we demonstrated that Exosomes derived from CMS-treated BMSCs inhibited osteoclastogenesis by attenuating NF- $\kappa$ B signaling pathway activity *in vitro* and ameliorated bone loss caused by mechanical unloading in an HU mouse model, providing new insights into intercellular communication between osteoblasts and osteoclasts under mechanical loading.

**Keywords:** Exosome; mechanical loading; bone marrow mesenchymal stem cell; osteoclast; osteoporosis

Submitted Mar 16, 2021. Accepted for publication May 08, 2021.

doi: 10.21037/atm-21-1838

View this article at: <http://dx.doi.org/10.21037/atm-21-1838>

## Introduction

Bone is a rigid but dynamic tissue that undergoes modeling and remodeling throughout life. Mechanical loading has been previously reported to play a crucial role in modulating bone remodeling and homeostasis (1-3). Under normal weight-bearing conditions, bone remodeling is coordinately regulated by osteoclastic bone resorption and osteoblastic bone formation. Reduced mechanical stimulation of bone disrupts this delicate equilibrium and leads to significant bone loss, as evidenced by disuse osteoporosis (DOP), which is a critical issue for long-term bed rest patients and astronauts (4-6).

Osteoblasts and osteoclasts, including their precursor cells, are sensitive to mechanical stimuli and can transform mechanical signals into biological responses (1,2,4-9). Proper mechanical stimulation promotes the osteogenic differentiation of bone marrow mesenchymal stem cells (BMSCs) through epigenetic regulation via HDAC1 and Dnmt3b (6,9). Our previous study demonstrated that mechanical loading positively regulates bone formation *in vivo* and that cyclic mechanical stretch (CMS) regulates osteoblast differentiation *in vitro* via mechanosensitive microRNA (miRNA)-103a directly targeting Runx2 (1). However, receptor activator of nuclear factor kappa-B ligand (RANKL)-induced osteoclast differentiation is directly suppressed during the period of mechanical loading but enhanced in the absence of mechanical stress (5,7,8). Previous studies have focused on the mechanical responses during the differentiation of osteoblasts and osteoclasts, but the intercellular communication between these cells under mechanical loading has not been fully elucidated.

Intercellular communication between osteoblasts and osteoclasts is important for the establishment and maintenance of bone remodeling (10-12). In addition, BMSCs not only act as progenitors of osteoblasts but also support osteoclast differentiation and participate in communication related to bone remodeling (13). Recently, exosomes, extracellular membrane vesicles with a diameter of ~30–160 nm, have been demonstrated to traffic RNA, DNA, and proteins between cells and serve as mediators of intercellular communication (14,15). Studies have

revealed multiple bone-derived exosomes participate in the regulation of bone homeostasis (13,14,16-19). For example, exosomes derived from UAMS-32P, an osteoblastic cell line, facilitate osteoclast formation (20). In contrast, osteoclast-derived miR-214-3p-containing exosomes can be transferred to osteoblasts to inhibit osteoblast activity and bone formation (10,21). To date, a large number of studies have confirmed that osteoclast-derived factors and exosome-packaged microRNAs (miRNAs) can either inhibit or enhance osteoblast differentiation through juxtacrine or paracrine mechanisms independent of their resorptive activity (17). However, research focusing on BMSC-derived exosomes influencing osteoclast differentiation is rare (18).

We hypothesized that exosomes play an important role in the maintenance of bone homeostasis through mediating intercellular communication between BMSCs and osteoclasts under mechanical loading. In this study, we demonstrated, for the first time, that exosomes derived from CMS-treated BMSCs (CMS\_Exos) strongly inhibited osteoclast differentiation by attenuating the nuclear factor kappa-B (NF- $\kappa$ B) signaling pathway. Furthermore, these exosomes effectively rescued osteoporosis caused by mechanical unloading in a hindlimb unloading (HU) mouse model *in vivo*. These results not only demonstrate the role of exosomes in communication between BMSCs and osteoclasts under mechanical loading, but also reveal a potential therapeutic approach for DOP.

We present the following article in accordance with the ARRIVE reporting checklist (available at <http://dx.doi.org/10.21037/atm-21-1838>).

## Methods

### Cell culture

The BMSCs were obtained from C57BL/6J mice and cultured as previously described (6). Briefly, BMSCs were flushed out of the femurs and tibiae with  $\alpha$ -minimum essential medium ( $\alpha$ -MEM) and cultured in growth medium ( $\alpha$ -MEM supplemented with 10% fetal bovine serum (FBS), 100 U/mL penicillin G, and 100  $\mu$ g/mL streptomycin (all from HyClone, Logan, UT, USA) at 37 °C in the presence

of 5% CO<sub>2</sub> after lysis of red blood cells. Nonadherent cells were removed by replacing the growth medium after 3 days. The attached BMSCs were not used beyond passage 5. Bone marrow macrophages (BMMs) were prepared as previously described (22). Briefly, cells extracted from the femurs and tibias of mice were allowed to proliferate in growth medium containing 30 ng/mL macrophage colony-stimulating factor [(M-CSF) R&D Systems, Minneapolis, MN, USA]. The cells were washed during a medium change to deplete residual stromal cells. At 80–90% confluence, the cells were washed with phosphate-buffered saline (PBS) 3 times and then trypsinized to harvest BMMs.

### *CMS application*

The BMSCs were seeded on 6-well flexible silicone rubber BioFlex plates coated with collagen type I (Flexcell International Corp., Hillsborough, NC, USA). The cells were cultured for 24–36 h to reach 60% confluency, at which time the growth medium was replaced. We applied CMS at a 0.5-Hz sinusoidal curve at 8% elongation using an FX-5000T Flexercell Tension Plus unit (Flexcell International Corp.) as described in our previous study (1). The cells were incubated in a humidified atmosphere at 37 °C and 5% CO<sub>2</sub> during stretching. The conditioned medium for exosome collection was supplemented with FBS which had been previously depleted of exosomes by ultracentrifugation at 120,000 g for 90 min. The culture supernatants were harvested immediately after 48 h of CMS stimulation. Control cells were cultured on the same plates in the same incubator but were not subjected to stretching.

### *Exosome extraction and identification*

Exosome extraction was performed as previously described (10). First, culture supernatant containing exosomes was harvested by centrifugation at 300 g for 10 min at 4 °C to remove floating cells, followed by additional rounds of centrifugation at 2,000 g for 20 min and 10,000 g for 5 min at 4 °C and passage through a 0.22 µm membrane filter to remove particles larger than 220 nm. At each step, the supernatant was transferred to new tubes, and the pellets were immediately rinsed with PBS. Exosomes were pelleted via ultracentrifugation at 120,000 g for 70 min at 4 °C, washed in PBS, ultracentrifuged again, and then the pellets were resuspended in PBS. The isolated exosomes were used immediately or stored at –80 °C. The protein concentration in exosomes was determined with a bicinchoninic (BCA) protein assay kit (Thermo Scientific, Waltham, MA, USA; Product

#23225). Exosome morphology was detected by transmission electron microscopy (TEM). The size distribution and intensity of exosomes were examined using NanoSight (NanoSight NS300, Malvern, UK). Specific exosomal biomarkers, including CD63 and TSG101, were detected by western blot analysis.

### *Exosome labeling and uptake*

The fluorescent dye 3,3'-dioctadecyloxycarbocyanine perchlorate (DiO) (Beyotime, Shanghai, China) was used to label exosomes and the cell membrane. The CMS\_Exos and exosomes derived from control BMSCs (static\_Exos) were incubated with the fluorescent dye DiO (5 mM) for 15 min at 37 °C, followed by 2 rounds of ultracentrifugation at 120,000 g for 90 min to remove any free dye. The labeled exosomes were incubated with BMMs for 4 h. After that, the cells were fixed and incubated with 4',6-diamidino-2-phenylidole ((DAPI) Beyotime, Shanghai, China) to stain cell nuclei. The uptake of labeled exosomes by BMMs was observed with an LSM5 confocal microscope (Zeiss, Oberkochen, Germany).

### *Measurement of cell viability and apoptosis*

The antiproliferative effect of exosomes on BMMs was assessed using a cell counting Kit-8 (CCK-8), according to the manufacturer's instructions. Briefly, BMMs were seeded and then cultured for 48 h with different doses of exosomes. Cell viability was examined using CCK-8 (Dojindo, Kumamoto, Japan). Optical density (OD) was measured at a wavelength of 450 nm (630 nm as reference) with an ELX800 microplate reader (Bio-Tek, Winooski, VT, USA). Detection of cell apoptosis rates was performed by flow cytometry using the FITC Annexin V Apoptosis Detection Kit I (BD Biosciences, San Jose, CA, USA). The BMMs were exposed to exosomes for 48 h in the presence or absence of RANKL. The results were analyzed with a FACStar (BD Biosciences). Nuclei were stained with DAPI in PBS at 37 °C for 10 min in the dark. The cell nuclei were observed and imaged with confocal microscopy.

### *In vitro osteoclastogenesis assay*

The BMMs were differentiated into osteoclasts over 5 days by incubation in complete culture medium containing RANKL (50 ng/mL) and M-CSF (30 ng/mL), as previously described (22). For determination of the influence of exosomes on osteoclast differentiation, exosomes were

included in the culture medium at a range of concentrations (0, 5, 10, or 25  $\mu\text{g}/\text{mL}$ ). Every other day during the incubation, the culture medium was replenished with fresh medium containing RANKL, M-CSF, and the indicated concentration of exosomes. For analysis of all stages of exosome addition-dependent effects on osteoclastogenesis, BMMs were cultured with exosomes (25  $\mu\text{g}/\text{mL}$ ) added at different stages of the 5-day culture period: days 0–2 (early stage) and days 3–5 (late stage). After 5 days, cells were fixed in paraformaldehyde and stained for tartrate-resistant acid phosphatase (TRAP) activity. The number of mature osteoclasts (TRAP<sup>+</sup> cells containing more than 3 nuclei) was calculated.

### *F-actin ring immunofluorescence*

For F-actin ring immunofluorescence staining, exosome-pretreated osteoclasts were fixed in 4% paraformaldehyde for 15 min, permeabilized in 0.1% Triton X-100 in PBS for 5 min, and then incubated with rhodamine-conjugated phalloidin for 30 min at room temperature. The cells were then incubated with DAPI for visualization of nuclei. The actin ring distribution was visualized using a confocal microscope.

### *Confocal microscopy for NF- $\kappa$ B localization*

The RAW264.7 cells were seeded in 6-well plates containing sterile cover slips. After incubation with culture medium at 37 °C for 24 h, the cells were pretreated with exosomes for 4 h, followed by stimulation with RANKL (50 ng/mL) for 20 min. After the incubation, the cells were washed twice with PBS, fixed in 4% paraformaldehyde for 20 min, and then permeabilized with 0.1% Triton X-100 for 30 min at room temperature. After blocking with 5% bovine serum albumin (BSA) for 1 h at room temperature, the cells were incubated with an anti-p65 subunit antibody (Cell Signaling Technology, Danvers, MA, USA) diluted 1:100 in PBS at 4 °C overnight. Nuclei were stained with DAPI. The nuclear translocation of p65 was imaged using confocal microscopy.

### *Western blot analysis*

Western blot analysis was performed as previously described (22). The RAW264.7 cells were seeded in 6-well plates at a density of  $6 \times 10^5$  cells per well. After growing to confluence, the cells were pretreated with or without

exosomes for 4 h. The cells were then stimulated with 50 ng/mL RANKL for 10 min. The cells were lysed with radioimmunoprecipitation assay (RIPA) lysis buffer (Thermo Fisher Scientific), and the protein concentration was determined with a BCA protein assay. Lysate proteins (30  $\mu\text{g}$ ) were separated by 10% sodium dodecyl sulfate polyacrylamide gel electrophoresis (SDS-PAGE) and transferred to polyvinylidene difluoride (PVDF) membranes. The membranes were blocked with 5% skim milk in tris-buffered saline with Tween 20 (TBST) for 1 h and incubated with primary antibodies overnight at 4 °C. A horseradish peroxidase (HRP)-conjugated secondary antibody was used at a 1:5,000 dilution. Immunoblots were visualized with an enhanced chemiluminescence detection system (Millipore, Billerica, MA, USA). Immunoreactive bands were quantified on scanned films in triplicate by normalizing the band intensities to the intensity of the glyceraldehyde 3-phosphate dehydrogenase (GAPDH) band with the help of Adobe Photoshop CS6 (Adobe Systems Incorporated, CA, USA). All primary antibodies and secondary antibodies used in this study were purchased from Cell Signaling Technology.

### *Hindlimb-unloading mice*

Animal studies were performed as previously described (1). Male 6-month-old C57BL/6J mice were purchased from Shanghai Laboratory Animal Co., Ltd. [(SLAC) Shanghai, China] and were individually caged under standard conditions (12 h light/12 h dark cycle, 21 °C controlled temperature). Animals were suspended from their hindlimbs for a period of 28 days. The suspension height was adjusted to prevent the hindlimbs from touching any supporting surface while maintaining a suspension angle of approximately 30 degrees. This allowed the forelimbs to have contact with the grid floor and allowed the animals to move around the cage for free access to food and water. Mice in the intervention groups received tail vein injections of static\_Exos or CMS\_Exos (5 mg/kg body weight, 0.1 mL per injection) twice a week for 4 weeks. In the weight-bearing (WB) group or HU group, the mice received an equal volume of PBS at the same time points. Every group has 10 mice. After 4 weeks, the bilateral femurs and tibiae were dissected and processed for micro-computed tomography ( $\mu\text{CT}$ ) examination and bone histomorphometric analysis. All animal experiments are approved by the Ethics Committee of Xinhua Hospital Ethics Committee Affiliated to Shanghai Jiao Tong

University School of Medicine (ID no: XHEC-D-2018-077 and XHEC-F-2018-025) and according to the National Institutes of Health in the Guide for the Care and Use of Laboratory Animals (NIH Publications No. 85-23, revised in 1996).

### *Micro computed tomography analysis of femurs*

Right femurs were fixed in 4% paraformaldehyde for 24 h and stored in 70% ethanol at 4 °C. The samples were scanned by high-resolution micro computed tomography ( $\mu$ CT) SCANCO  $\mu$ CT 100, Brüttisellen, Switzerland). Each femur was imaged with the following instrument settings: 70 kV, 200  $\mu$ A, 0.5 mm Al filter, 300 ms exposure, and 10  $\mu$ m pixel size. After scanning, the data were reconstructed with SCANCO  $\mu$ 100 Evaluation V6.5-3 with a constant threshold value. The region of interest (ROI) of trabecular bone was 0.8 mm in height and 0.3 mm below the growth plate, and the ROI of cortical bone was 1 mm in height and 2 mm below the growth plate. The ROI of bone within this volume was manually defined, and the following bone parameters were included: trabecular thickness (Tb.Th), bone mineral density (BMD), bone volume percentage (BV/TV), trabecular number (Tb.N), trabecular separation (Tb.Sp), and cortical thickness (Ct.Th).

### *Histological and histomorphometric analysis*

Left femurs were fixed in 4% paraformaldehyde for 24 h, and then 12.5% ethylenediamine tetraacetic acid (EDTA) was used for decalcification for approximately 3 weeks. The tissues were embedded in paraffin, and histological sections (5  $\mu$ m thick) were made. Subsequently, the sections underwent hematoxylin and eosin (H&E) and TRAP staining with methyl green counterstaining. A high-quality microscope was used to examine and image the specimens. The number of TRAP<sup>+</sup> multinucleated osteoclasts (N.Oc/BS, 1/mm) and the percentage of osteoclast surface per bone surface (OcS/BS, %) were assessed for each sample.

### *Statistical analysis*

The software SPSS 22.0 software (SPSS Inc., Armonk, NY, USA) was used for statistical analysis. All values are presented as the mean  $\pm$  standard deviation (SD) of 3 independent replicates. Student's *t*-test was performed to compare differences. Significant differences were indicated by  $P < 0.05$  and  $P < 0.01$ .

## **Results**

### *Characterization of exosomes and incorporation of exosomes into BMMs*

Exosomes were successfully isolated from BMSC culture medium and identified (*Figure 1*). The exosomes were observed using TEM, revealing a typical diameter of ~100–150 nm with a rounded morphology (*Figure 1A*). Particle size and concentration were measured by NanoSight (Malvern Panalytical, Malvern, UK) (*Figure 1B*). The diameters of static\_Exos were distributed at 60–200 nm with a size peak of 98 nm, and the diameters of CMS\_Exos were distributed at 40–260 nm with a size peak of 105 nm. Western blot analysis results confirmed the presence of expected proteins, such as CD63 and TSG101, in the exosomes, and the absence of the nuclear proteins LaminA/C and the endoplasmic reticulum protein Calnexin (*Figure 1C*).

To assess whether exosomes derived from BMSCs can be internalized by BMMs, exosomes were labeled with DiO (green). The labeled exosomes were incubated with BMMs for 4 h at 37 °C. The cells were then observed by confocal microscopy, which revealed the incorporation of exosomes into BMMs (*Figure 1D*).

### *CMS\_Exos inhibit RANKL-induced osteoclastogenesis and actin ring formation*

To examine the effects of exosomes derived from BMSCs on RANKL-induced osteoclastogenesis *in vitro*, a cell viability test was performed first. Concentrations of up to 50  $\mu$ g/mL static\_Exos or CMS\_Exos had no cytotoxic effects on BMMs which had been treated with static\_Exos or CMS\_Exos for 48 h. The BMMs were treated with M-CSF and RANKL in the absence or presence of different concentrations of exosomes for 5 days. Numerous TRAP<sup>+</sup> multinucleated osteoclasts were formed under stimulation with M-CSF and RANKL, whereas osteoclast formation was inhibited by CMS\_Exo treatment in a dose-dependent manner (*Figure 2A,B*). However, static\_Exo treatment showed no significant inhibitory effect on osteoclast formation (*Figure 2A,B*). To examine the stage at which CMS\_Exos inhibited osteoclastogenesis, we added 25  $\mu$ g/mL exosomes to the culture medium at 0 or 3 days during osteoclast differentiation. The CMS\_Exo treatment during the early stage (days 0–2) significantly suppressed osteoclastogenesis (*Figure 2C,D*). Furthermore, exposure of osteoclastic precursor cells to CMS\_Exos during the later stage (days 3–5) also affected osteoclast formation, but the

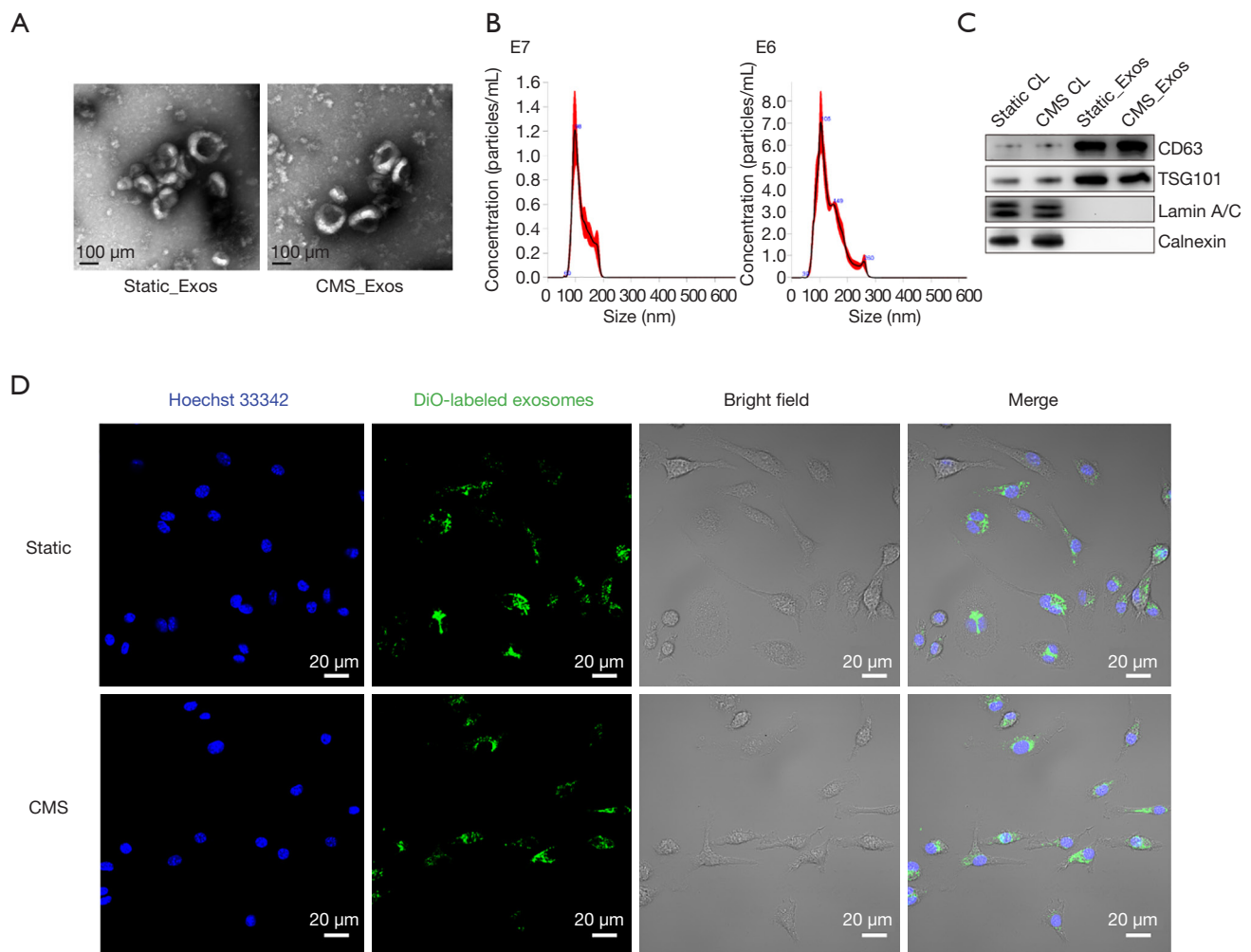


**Figure 1** Characterization of exosomes and incorporation of exosomes into BMMs. (A) Electron microscopy images of exosomes. Scale bar, 100 nm. (B) The size distribution and concentration of exosomes secreted by BMSCs measured by nanoparticle tracking analysis. (C) Western blotting for the exosomal markers CD63 and TSG101, nuclear proteins LaminA/C and the endoplasmic reticulum protein Calnexin. (D) Confocal microscopy images showing the colocalization of exosomes from BMSCs with BMMs. Exosomes were labeled with DiO (green), and BMM cell nuclei were stained with Hoechst 33342 (blue). BMM, bone marrow macrophage; BMSCs, bone marrow mesenchymal stem cells; DiO, 3,3'-dioctadecyloxycarbocyanine perchlorate.

effect was weaker than that of treatment during the early stage (Figure 2C,D). Thus, CMS\_Exos inhibited osteoclast differentiation during both the early and late stages.

The F-actin rings are an important constituent of osteoclasts and a prerequisite for efficient bone resorption. Thus, we further assessed the effect of CMS\_Exos on F-actin ring formation. Clear actin ring structures were observed in the vehicle treatment group and static\_Exo group (Figure 2E). However, the actin ring structure was almost completely disrupted when BMMs were incubated with 25  $\mu\text{g}/\text{mL}$  CMS\_Exos (Figure 2E,F).

To exclude the possibility that exosomes induced BMM apoptosis during differentiation, BMMs were treated with static\_Exos or CMS\_Exos in the absence or presence of RANKL for 48 h. The number of Annexin-V + cells was evaluated by flow cytometry. The BMMs treated with CMS\_Exos at a concentration of 25  $\mu\text{g}/\text{mL}$  showed suppressed osteoclast formation, but the number of Annexin-V + BMMs was not affected by CMS\_Exo treatment at 48 h compared with control treatment (Figure 3A,B,C). Furthermore, BMMs stained with DAPI exhibited normal intact nuclei after CMS\_Exo treatment (Figure 3D,E), thereby confirming that the

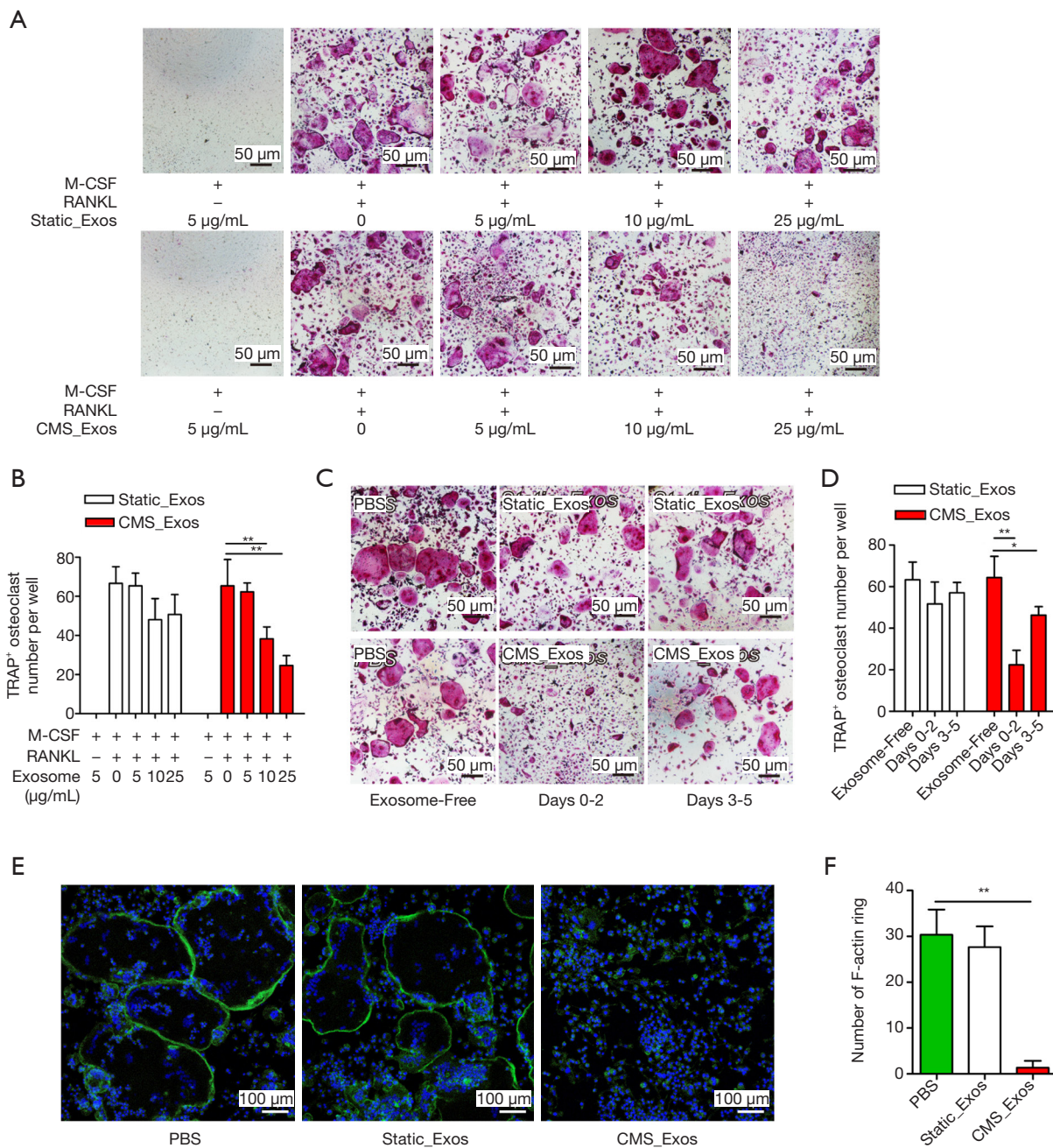


**Figure 2** CMS\_Exos inhibit RANKL-induced osteoclastogenesis and actin ring formation. (A) Representative images of RANKL-stimulated BMMs stained for TRAP (red) after treatment with the indicated exosomes at different concentrations (0, 5, 10, or 25 µg/mL). (B) The number of TRAP-positive multinucleated osteoclasts ( $\geq 3$  nuclei) was quantified. (C) Effect of the time of indicated exosome addition on osteoclast formation. BMM cells were stimulated with RANKL (50 ng/mL) alone or cotreated with the indicated exosomes (25 µg/mL) at different stages during a 5-day osteoclast culture. The cells were fixed and stained for TRAP activity. (D) The number of TRAP-positive multinucleated osteoclasts ( $\geq 3$  nuclei) was quantified. (E) BMMs were stimulated with RANKL and the indicated exosomes until mature osteoclasts formed. Then, the cells were fixed and stained for F-actin. The actin ring distribution was visualized by confocal microscopy. (F) The number of osteoclasts with an intact actin ring was counted. All experiments were performed at least 3 times, and representative images are shown. Data are expressed as the mean  $\pm$  SD; \* $P < 0.05$ , \*\* $P < 0.01$ . CMS\_Exos, CMS-treated BMSC-derived exosomes; RANKL, receptor activator of nuclear factor kappa-B ligand; BMM, bone marrow macrophage; TRAP, tartrate-resistant acid phosphatase; SD, standard deviation.

inhibitory effects of CMS\_Exos on osteoclastogenesis were not caused by the induction of BMM apoptosis.

### ***CMS\_Exos inhibit RANKL-induced activation of the NF- $\kappa$ B signaling pathway***

Activation of the NF- $\kappa$ B signaling pathway plays a crucial role in osteoclastogenesis. To further explore the underlying mechanisms through which CMS\_Exos regulate osteoclast formation, we investigated RANKL-induced signaling pathways. To directly observe the impact of exosomes on NF- $\kappa$ B signaling, immunofluorescence staining was performed to analyze the nuclear translocation of NF- $\kappa$ B/p65 (Figure 4A). Negative control cells were not exposed to RANKL or exosomes. These results clearly showed that compared with the negative control cells, RANKL-stimulated Raw264.7 cells displayed obvious translocation of p65 (red) from the cytoplasm to nucleus (blue), and that this translocation could be prevented by CMS\_Exos. However, static\_Exos did not affect p65 translocation. Furthermore, western blotting revealed changes in NF- $\kappa$ B pathway protein levels (Figure 4B,C). Some NF- $\kappa$ B pathway-related proteins, including inhibitor of NF- $\kappa$ B inhibitor  $\alpha$  (I $\kappa$ B $\alpha$ ), I $\kappa$ B kinase (IKK), and p65, were phosphorylated or activated under RANKL stimulation. The degradation of I $\kappa$ B $\alpha$  allows activated NF- $\kappa$ B/p65 to translocate into the nucleus and regulate the expression of certain genes. However, this process was inhibited effectively by CMS\_Exos but not by static\_Exos (Figure 4C). Additionally, the phosphorylation of IKK $\alpha/\beta$  was suppressed by CMS\_Exos but not by static\_Exos in the context of RANKL stimulation (Figure 4C). Therefore, the inhibitory effects of CMS\_Exos on NF- $\kappa$ B signaling may play a pivotal role in the inhibition of RANKL-stimulated osteoclastogenesis.

### ***CMS\_Exos prevented HU-induced bone loss***

To evaluate the role of exosomes in DOP, we established an HU-induced bone loss mouse model. There were no fatalities during HU treatment or exosome administration. Through  $\mu$ CT, it was confirmed that there was significant loss of femur trabecular and cortical bone in HU mice, which was indicated by decreased BMD, BV/TV, Tb.Th, Tb.N, and Ct.Th values as well as an increased Tb.Sp value for HU mice compared to WB mice (Figure 5A,B). However, the extent of trabecular bone loss was significantly suppressed by treatment with CMS\_Exos. The relative bone loss in mice treated with CMS\_Exos compared with that in HU mice treated with

the vehicle was markedly less than that in the mice treated with static\_Exos (Figure 5A,B). Cortical bone loss was ameliorated by treatment with CMS\_Exos but not static\_Exos, indicating that CMS\_Exos had a more comprehensive antiosteoporosis function. In agreement with the  $\mu$ CT analysis results, histological H&E-stained sections revealed that the trabeculae in regions proximal and distal to the growth plate were thin in the HU mouse group (Figure 5C). In contrast, HU mice treated with CMS\_Exos exhibited a dramatic increase in bone density and marked increases in trabecular density and thickness compared with HU mice treated with the vehicle (Figure 5C).

To further explore whether osteoclasts are involved in the inhibitory effects of exosomes on HU-induced bone loss, we performed TRAP staining on femur bone sections. Accordingly, TRAP staining revealed a significant decrease in the numbers of TRAP+ multinucleated cells at the growth plates and trabecular surface of CMS\_Exo-treated mice compared with vehicle-treated HU mice (Figure 5C). Moreover, histomorphometric analysis of Oc.S/BS and the number of osteoclasts confirmed that CMS\_Exo treatment attenuated HU-induced bone loss and reduced osteoclast numbers (Figure 5D). Although static\_Exo treatment rescued trabecular bone loss in mice to a certain extent, it did not show significant inhibition of osteoclasts *in vivo*, manifesting as no significant reductions in the number or area of osteoclasts on the bone surface (Figure 5C,D). Collectively, these results indicated that CMS\_Exos effectively prevented HU-induced bone loss *in vivo*.

## **Discussion**

It has been proposed that BMSCs are promising candidates for the treatment of various diseases, such as those of muscle, bone, and cartilage; blood-related diseases; immune system diseases; nervous system diseases; and injuries (23). Recently, it was identified that BMSCs exert their therapeutic activity through a paracrine effect mediated by the release of small extracellular vesicles (EVs) (16). Exogenous BMSC-EVs can be taken up and promote the osteogenic differentiation of endogenous BMSCs (24). Moreover, BMSC-EVs can be endocytosed by osteoblasts and release their cargo into target cells to positively regulate osteogenic genes and osteoblastic differentiation (25). However, studies focusing on BMSC-derived exosomes influencing osteoclast differentiation are rare (18). In this study, we investigated the effects of exosomes derived from static or mechanically stimulated BMSCs on osteoclast

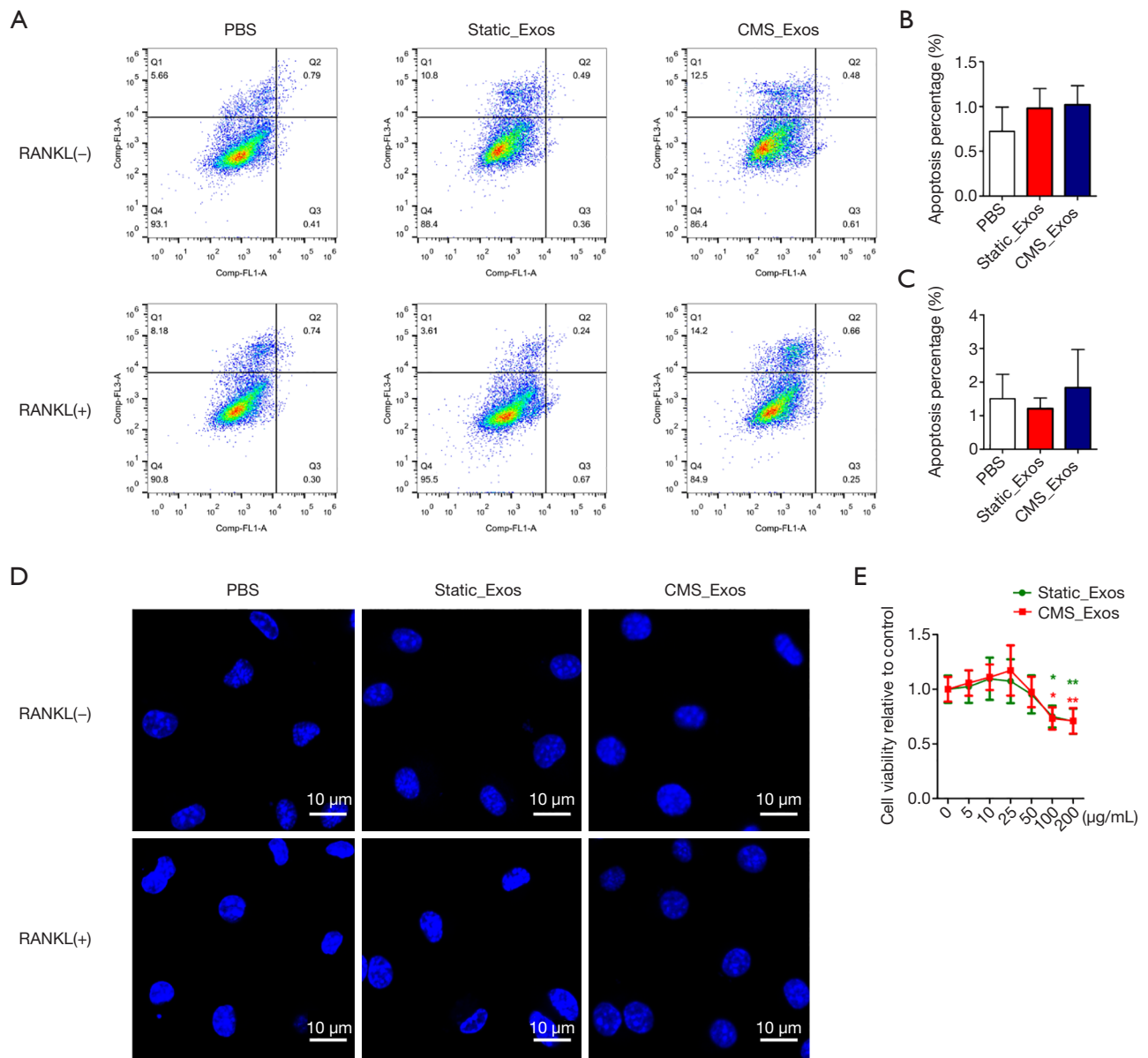


**Figure 3** Exosomes do not affect BMM cell viability or induce cell apoptosis at low concentrations. (A) Flow cytometry analysis of the apoptosis rate of BMMs treated with 25  $\mu\text{g/mL}$  exosomes for 48 h. Quantitative analysis of the apoptosis rates of BMMs (B) not stimulated with RANKL or (C) stimulated with RANKL. (D) Exosomes did not induce nuclear fragmentation. BMMs were treated with the indicated exosomes for 48 h before the cells were fixed, stained with 0.1  $\mu\text{g/mL}$  DAPI, and examined by fluorescence microscopy. (E) CCK-8 assay performed to analyze the cell viability of BMMs incubated with the indicated exosomes for 48 h. All experiments were performed at least 3 times, and representative images are shown. Data are expressed as the mean  $\pm$  SD; \* $P < 0.05$ , \*\* $P < 0.01$ . BMM, bone marrow macrophage; RANKL, receptor activator of nuclear factor kappa-B ligand; DAPI, 4',6-diamidino-2-phenylidole; CCK-8, Cell Counting Kit-8; SD, standard deviation.

differentiation. The results indicated that CMS\_Exos effectively inhibited RANKL-induced osteoclastogenesis by attenuating the NF- $\kappa$ B signaling pathway *in vitro*.

Moreover, CMS\_Exos rescued osteoporosis in a mechanical unloading mouse model *in vivo*.

Mechanical stimulation has been reported as an

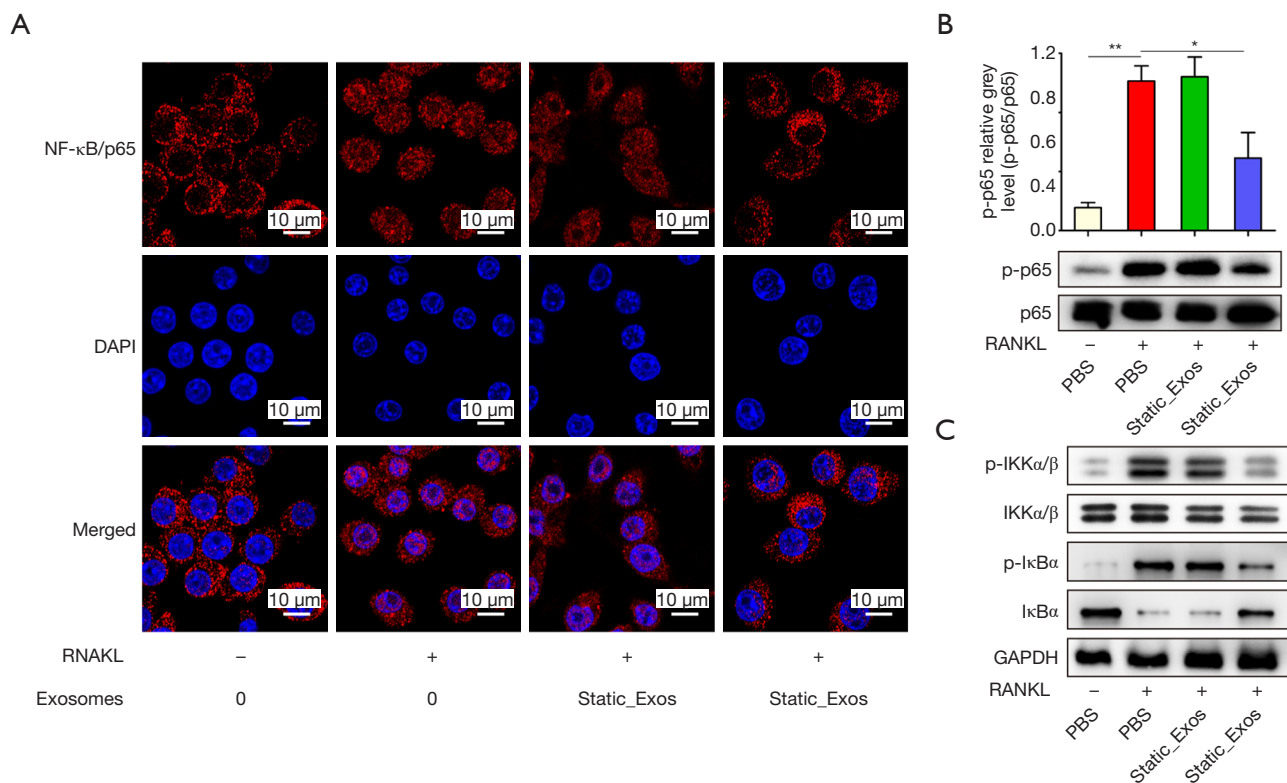
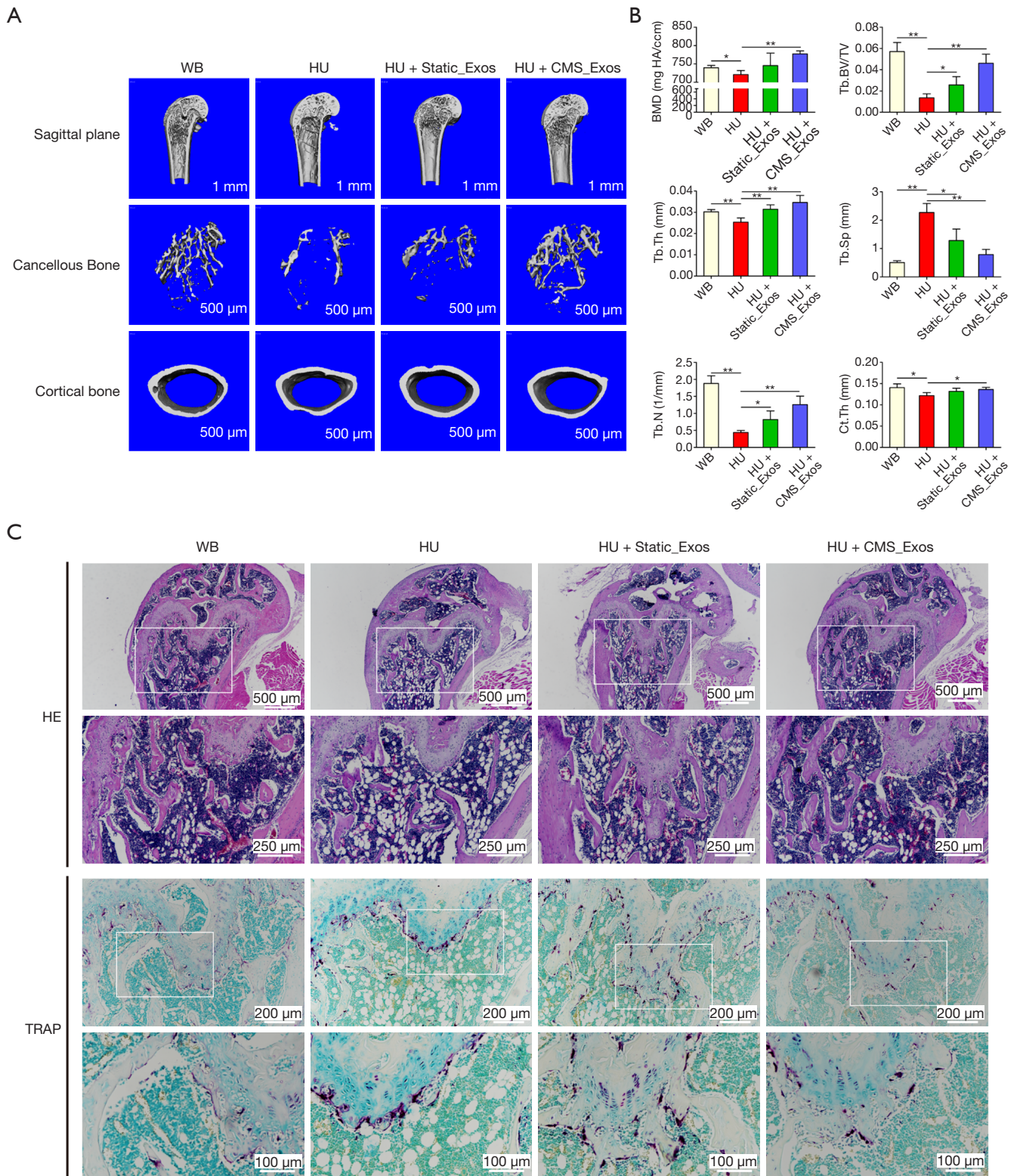


**Figure 4** CMS\_Exos inhibit the RANKL-induced activation of the NF-κB signaling pathway. (A) RAW264.7 cells were treated with the indicated exosomes for 4 h, followed by stimulation with RANKL (50 ng/mL) for 20 min. The localization of p65 was visualized by immunofluorescence staining. (B,C) Western blot analysis of the levels of the indicated proteins in BMMs pretreated with or without exosomes for 4 h prior to RANKL stimulation (50 ng/mL). The bar graph in (B) shows the relative expression of p-p65 calculated from the band intensity using ImageJ software. All experiments were performed at least 3 times, and representative images are shown. Data are expressed as the mean  $\pm$  SD; \* $P$ <0.05, \*\* $P$ <0.01. CMS\_Exos, CMS-treated BMSC-derived exosomes; RANKL, receptor activator of nuclear factor kappa-B ligand; NF-κB, nuclear factor-kappa B; BMM, bone marrow macrophage; SD, standard deviation.

important regulator in diverse biological and pathological processes, including affecting the secretion of EVs and their cargoes (1,4,26,27). Recently, studies have shown that both cyclic and continuous stretching regulate the expression of specific miRNAs in EVs in lung epithelial cells and regulate lung development (26). Exosomes from cyclic stretch-treated periodontal ligament cells contribute to the maintenance of periodontal immune/inflammatory homeostasis by inhibiting interleukin 1 $\beta$  (IL-1 $\beta$ ) production and pyroptosis in macrophages (27). In the present study, we characterized exosomes secreted by static culture- or mechanical stretch-treated BMSCs. The uptake of these exosomes by BMMs was observed by confocal microscopy, confirming a direct interaction between BMSC-derived exosomes and BMMs. Neither the indicated concentration of CMS\_Exos nor that of static\_Exos affected the

apoptosis of BMMs in the presence or absence of RANKL. Interestingly, CMS\_Exo treatment produced sustained osteoclast differentiation inhibition, while static\_Exo treatment did not, indicating that mechanical stimulation altered the cargo profile of BMSC-derived exosomes. To our knowledge, this is the first report about the effects of BMSC-derived exosomes on osteoclast differentiation.

During osteoclast differentiation, RANKL binding to RANK induces the activation of several vital signaling pathways. As an essential signaling pathway in most cells, the strong activation of NF-κB by RANKL plays a crucial role in osteoclast differentiation, resorption function, and survival (28). Thus, we investigated the RANKL-induced changes in the levels of proteins involved in NF-κB signaling in this study. When BMMs are stimulated with RANKL, IκB is phosphorylated by the IκB kinase complex



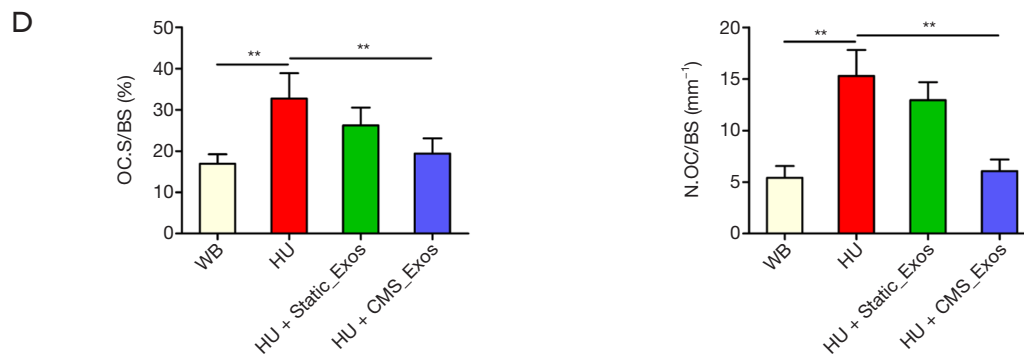


**Figure 5** CMS\_Exos prevented HU-induced bone loss. (A) Representative reconstructed micro-CT images of the distal femur in the indicated group. n=5. (B) Three-dimensional microstructural parameters of the distal femur in the indicated group. (C) Representative H&E and TRAP staining images of the distal femur showing the bone volume in the indicated group. n=5. (D) The percentage of osteoclast surface per bone surface (OcS/BS, %) and number of osteoclasts per field of tissue (No. of OCs per field) at 200× magnification were analyzed. Data are expressed as the mean ± SD; \*P<0.05, \*\*P<0.01. CMS\_Exos, CMS-treated BMSC-derived exosomes; HU, hindlimb unloading; micro-CT, micro computed tomography; H&E, hematoxylin-eosin; TRAP, tartrate-resistant acid phosphatase; SD, standard deviation.

[IKK $\alpha$ , IKK $\beta$ , and NK-kappa-B essential modulator (NEMO)], ubiquitinated, and degraded by the ubiquitin-proteasome system. Then, free NF- $\kappa$ B proteins (such as p65) translocate into the nucleus and recognize DNA target sites to trigger the expression of osteoclastogenesis-related genes (29). However, it was found that the degradation of I $\kappa$ B $\alpha$  and phosphorylation of p65, IKK $\alpha$ / $\beta$ , and I $\kappa$ B $\alpha$  were effectively blocked by CMS\_Exo exposure but not by static\_Exo exposure. Moreover, immunofluorescence analysis showed that CMS\_Exos disturbed p65 nuclear translocation, thus preventing the activation of downstream factors. In short, CMS\_Exos attenuated osteoclast formation and function via inhibition of the NF- $\kappa$ B signaling pathway.

Increasing evidence has shown the therapeutic potential of exosomes in treating various bone diseases (30,31). The BMD of bovine colostrum exosome-fed glucocorticoid-induced osteoporosis mice was significantly improved compared with that of control mice without exosome treatment (32). In a femoral fracture model, mice treated with exosomes from human umbilical cord MSCs (HUCMSCs) cultured under hypoxic conditions showed a significantly larger callus volume and greater vascularity in the fracture site than those treated with exosomes from HUCMSCs cultured under normoxic conditions or with PBS (33). Recently, exosomes derived from HUCMSCs were shown to have therapeutic effects on a rat DOP model (34); however, this study only focused on the apoptosis of BMSCs and did not investigate the biological behavior of osteoclasts and the intercellular communication between BMSCs and osteoclasts.

Mechanical signals play critical roles in bone growth and homeostasis (35,36), and we hypothesized that exosomes play a pivotal role in the maintenance of bone homeostasis through mediating intercellular communication between BMSCs and osteoclasts under mechanical loading. Indeed, static\_Exos decreased bone loss to a certain extent. The bone loss in the mice treated with CMS\_Exos was markedly less than that compared with that in the HU mice treated with the vehicle. Moreover, cortical bone loss was ameliorated by treatment with CMS\_Exos but not static\_Exos. This may be because mechanical stimulation changes the components of exosome cargoes, which makes special exosomes exhibit superior anti-DOP activity. It is not clear which component is responsible for this effect, and further investigations identifying the specific content and exploring the underlying molecular mechanisms are needed to optimize the efficacy of CMS\_Exos for DOP therapy.

## Conclusions

In summary, our study has provided new insights into intercellular communication between osteoblasts and osteoclasts under mechanical loading. Exosomes derived from CMS-treated BMSCs suppressed osteoclastogenesis by attenuating NF- $\kappa$ B signaling pathway activity *in vitro* and ameliorated bone loss caused by mechanical unloading in an HU mouse model. In-depth studies on CMS\_Exo components, such as proteins and miRNAs, are required to understand how CMS\_Exos function at the molecular level.

## Acknowledgments

*Funding:* This study was sponsored by Shanghai Sailing Program (20YF1429100), Shanghai Natural Science Fund (19ZR1433100), Interdisciplinary of Medicine and Engineering Foundation of Shanghai Jiao Tong University (YG2019ZDA22), Biomedical Technology Support Program of Shanghai (20S31900200).

## Footnote

*Reporting Checklist:* The authors have completed the ARRIVE reporting checklist. Available at <http://dx.doi.org/10.21037/atm-21-1838>

*Data Sharing Statement:* Available at <http://dx.doi.org/10.21037/atm-21-1838>

*Conflicts of Interest:* All authors have completed the ICMJE uniform disclosure form (available at <http://dx.doi.org/10.21037/atm-21-1838>). The authors have no conflicts of interest to declare.

*Ethical Statement:* The authors are accountable for all aspects of the work in ensuring that questions related to the accuracy or integrity of any part of the work are appropriately investigated and resolved. The experimental processes were approved by the Ethics Committee of Xinhua Hospital Ethics Committee Affiliated to Shanghai Jiao Tong University School of Medicine (ID no: XHEC-D-2018-077 and XHEC-F-2018-025) and according to the National Institutes of Health in the Guide for the Care and Use of Laboratory Animals (NIH Publications No. 85-23, revised in 1996).

*Open Access Statement:* This is an Open Access article distributed in accordance with the Creative Commons Attribution-NonCommercial-NoDerivs 4.0 International License (CC BY-NC-ND 4.0), which permits the non-commercial replication and distribution of the article with the strict proviso that no changes or edits are made and the original work is properly cited (including links to both the formal publication through the relevant DOI and the license). See: <https://creativecommons.org/licenses/by-nc-nd/4.0/>.

## References

- Zuo B, Zhu JF, Li J, et al. microRNA-103a functions as a mechanosensitive microRNA to inhibit bone formation through targeting Runx2. *J Bone Miner Res* 2015;30:330-45.
- Hsieh YF, Turner CH. Effects of loading frequency on mechanically induced bone formation. *J Bone Miner Res* 2001;16:918-24.
- Yan Y, Wang LP, Ge LH, et al. Osteocyte-Mediated Translation of Mechanical Stimuli to Cellular Signaling and Its Role in Bone and Non-bone-Related Clinical Complications. *Curr Osteoporos Rep* 2020;18:67-80.
- Li J, Wan Z, Liu H, et al. Osteoblasts subjected to mechanical strain inhibit osteoclastic differentiation and bone resorption in a co-culture system. *Ann Biomed Eng* 2013;41:2056-66.
- Nabavi N, Khandani A, Camirand A, et al. Effects of microgravity on osteoclast bone resorption and osteoblast cytoskeletal organization and adhesion. *Bone* 2011;49:965-74.
- Wang C, Shan S, Wang C, et al. Mechanical stimulation promote the osteogenic differentiation of bone marrow stromal cells through epigenetic regulation of Sonic Hedgehog. *Exp Cell Res* 2017;352:346-56.
- Suzuki N, Yoshimura Y, Deyama Y, et al. Mechanical stress directly suppresses osteoclast differentiation in RAW264.7 cells. *Int J Mol Med* 2008;21:291-6.
- Kadow-Romacker A, Hoffmann JE, Duda G, et al. Effect of mechanical stimulation on osteoblast- and osteoclast-like cells in vitro. *Cells Tissues Organs* 2009;190:61-8.
- Wang J, Wang CD, Zhang N, et al. (2016). Mechanical stimulation orchestrates the osteogenic differentiation of human bone marrow stromal cells by regulating HDAC1. *Cell Death Dis* 7:e2221.
- Sun W, Zhao C, Li Y, et al. Osteoclast-derived microRNA-containing exosomes selectively inhibit osteoblast activity. *Cell Discov* 2016;2:16015.
- Yuan FL, Wu QY, Miao ZN, et al. Osteoclast-Derived Extracellular Vesicles: Novel Regulators of Osteoclastogenesis and Osteoclast-Osteoblasts Communication in Bone Remodeling. *Front Physiol* 2018;9:628.
- Park YE, Musson D, Naot D, et al. Cell-cell communication in bone development and whole-body homeostasis and pharmacological avenues for bone disorders. *Curr Opin Pharmacol* 2017;34:21-35.
- Liu J, Li D, Wu X, et al. Bone-derived exosomes. *Curr Opin Pharmacol* 2017;34:64-9.
- Yin P, Lv H, Li Y, et al. Exosome-Mediated Genetic Information Transfer, a Missing Piece of Osteoblast-Osteoclast Communication Puzzle. *Front Endocrinol (Lausanne)* 2017;8:336.

15. Kalluri R, LeBleu VS. The biology, function, and biomedical applications of exosomes. *Science* 2020;367:eaau6977.
16. Liu M, Sun Y, Zhang Q. Emerging Role of Extracellular Vesicles in Bone Remodeling. *J Dent Res* 2018;97:859-68.
17. Zhu S, Yao F, Qiu H, et al. Coupling factors and exosomal packaging microRNAs involved in the regulation of bone remodelling. *Biol Rev Camb Philos Soc* 2018;93:469-80.
18. Li Y, Jin D, Xie W, et al. Mesenchymal Stem Cells-Derived Exosomes: A Possible Therapeutic Strategy for Osteoporosis. *Curr Stem Cell Res Ther* 2018;13:362-8.
19. Vitha AE, Kollefath AW, Huang CC, et al. Characterization and Therapeutic Uses of Exosomes: A New Potential Tool in Orthopedics. *Stem Cells Dev* 2019;28:141-50.
20. Deng L, Wang YP, Peng Y, et al. Osteoblast-derived microvesicles: A novel mechanism for communication between osteoblasts and osteoclasts. *Bone* 2015;79:37-42.
21. Ota S, Zhou ZQ, Romero MP, et al. HDAC6 deficiency or inhibition blocks FGFR3 accumulation and improves bone growth in a model of achondroplasia. *Hum Mol Genet* 2016;25:4227-43.
22. Xiao F, Zhai Z, Jiang C, et al. Geraniin suppresses RANKL-induced osteoclastogenesis in vitro and ameliorates wear particle-induced osteolysis in mouse model. *Exp Cell Res* 2015;330:91-101.
23. Chu DT, Phuong T, Tien NB, et al. An Update on the Progress of Isolation, Culture, Storage, and Clinical Application of Human Bone Marrow Mesenchymal Stem/Stromal Cells. *Int J Mol Sci* 2020;21:e708.
24. Liu S, Liu DW, Chen CD, et al. MSC Transplantation Improves Osteopenia via Epigenetic Regulation of Notch Signaling in Lupus. *Cell Metab* 2015;22:606-18.
25. Qin Y, Wang L, Gao Z, et al. Bone marrow stromal/stem cell-derived extracellular vesicles regulate osteoblast activity and differentiation in vitro and promote bone regeneration in vivo. *Sci Rep* 2016;6:21961.
26. Najrana T, Mahadeo A, Abu-Eid R, et al. Mechanical stretch regulates the expression of specific miRNA in extracellular vesicles released from lung epithelial cells. *J Cell Physiol* 2020;235:8210-23.
27. Wang Z, Maruyama K, Sakisaka Y, et al. Cyclic Stretch Force Induces Periodontal Ligament Cells to Secrete Exosomes That Suppress IL-1 $\beta$  Production Through the Inhibition of the NF- $\kappa$ B Signaling Pathway in Macrophages. *Front Immunol* 2019;10:1310.
28. Jiang C, Xiao F, Gu X, et al. Inhibitory effects of ursolic acid on osteoclastogenesis and titanium particle-induced osteolysis are mediated primarily via suppression of NF-kappaB signaling. *Biochimie* 2015;111:107-18.
29. Jimi E, Takakura N, Hiura F, et al. The Role of NF- $\kappa$ B in Physiological Bone Development and Inflammatory Bone Diseases: Is NF- $\kappa$ B Inhibition "Killing Two Birds with One Stone"? *Cells* 2019;8:1636.
30. Tan SH, Wong J, Sim S, et al. Mesenchymal stem cell exosomes in bone regenerative strategies-a systematic review. *Mater Today Bio* 2020;7:100067.
31. Zuo R, Liu M, Wang Y, et al. BM-MSD-derived exosomes alleviate radiation-induced bone loss by restoring the function of recipient BM-MSCs and activating Wnt/ $\beta$ -catenin signaling. *Stem Cell Res Ther* 2019;10:30.
32. Yun B, Maburutse B, Kang M, et al. Short communication: Dietary bovine milk-derived exosomes improve bone health in an osteoporosis-induced mouse model. *J Dairy Sci* 2020;103:7752-60.
33. Liu W, Li L, Rong Y, et al. Hypoxic mesenchymal stem cell-derived exosomes promote bone fracture healing by the transfer of miR-126. *Acta Biomater* 2020;103:196-212.
34. Yang BC, Kuang M, Kang J, et al. Human umbilical cord mesenchymal stem cell-derived exosomes act via the miR-1263/Mob1/Hippo signaling pathway to prevent apoptosis in disuse osteoporosis. *Biochem Biophys Res Commun* 2020;524:883-9.
35. Grimm D, Grosse J, Wehland M, et al. The impact of microgravity on bone in humans. *Bone* 2016;87:44-56.
36. Li X, Han L, Nookaew I, et al. Stimulation of Piezo1 by mechanical signals promotes bone anabolism. *eLife* 2019;8:e49631.

**Cite this article as:** Xiao F, Zuo B, Tao B, Wang C, Li Y, Peng J, Shen C, Cui Y, Zhu J, Chen X. Exosomes derived from cyclic mechanical stretch-exposed bone marrow mesenchymal stem cells inhibit RANKL-induced osteoclastogenesis through the NF- $\kappa$ B signaling pathway. *Ann Transl Med* 2021;9(9):798. doi: 10.21037/atm-21-1838